RSC Advances

ROYAL SOCIETY OF CHEMISTRY

www.rsc.org/advances

RSC Advances

RSCPublishing

COMMUNICATION

Novel Field Emission Structure of CuO/Cu_2O Composite Nanowires Based on Copper Through Silicon Via Technology

Cite this: DOI: 10.1039/x0xx00000x

Received ooth January 2014,
Accepted ooth January 2014

DOI: 10.1039/x0xx00000x

www.rsc.org/

Cheng-Liang Hsu* [a], Jia-Yu Tsai[a], Ting-Jen Hsueh*[b]

A novel Cu through silicon via (TSV) fabrication process that does not require chemical mechanical polishing, temporary bonding, and de-bonding processes was developed. The Cu TSV has a square pattern with a side length of ~80 µm and a depth of ~280 µm. Uniform, high-density CuO/Cu_2O composite nanowires (NWs) were grown on the Cu TSV using thermal oxidation. The field emission turn-on field and enhancement factor of the CuO/Cu_2O composite NWs were 4.7 V/µm and ~2902, respectively.

Introduction

Cupric oxide (CuO) and cuprous oxide (Cu_2O) are p-type semiconductors with monoclinic and cubic crystalline structures, respectively. It is well known that CuO and Cu_2O are photovoltaic materials due to their narrow direct bandgap (~1.2 and ~2.1 eV, respetively) at room temperature.[1-2] CuO one-dimensional (1D) nanostructures (NSs) have attracted a lot of attention for applications such as solar cells,[3] gas sensors,[4] humidity sensors,[5] high-temperature superconductors,[6] and field emitters.[7] For these applications, CuO is a suitable field emitter due to its relatively small bandgap and good conductivity compared to those of other metal oxide materials. CuO 1D NSs have a high length-to-diameter ratio (aspect ratio), giving them a large enhancement factor and low turn-on electric field. Various methods have been used to synthesize CuO 1D NSs, including vapor-liquid-solid (VLS) growth,[8] chemical vapor deposition (CVD),[9] solution-phase synthesis,[10] and the heating of Cu foil and Cu3N or Cu thin film.[11-22]

Integrated circuit (IC) fabrication techniques will face physical limitation challenges when the CMOS gate length is downscaled to 7 nm and beyond.[23] Three-dimensional (3D) stacked IC fabrication technology can overcome the scale limit by using through silicon via (TSV) technology. TSV technology can enhance the performance of 3D ICs. A lot of effort has been devoted to simplifying the TSV process to increase stability and reduce cost. For example, Kim et al. proposed a without handle carrier process for high-frequency applications.[24] Chen et al. proposed an approach for sealing bump bottom-up Cu TSV plating,[25-26] which simplifies the handle carrier and the polishing process of Cu. The present study develops a simple top-down Cu TSV plating approach that uses an etching barrier layer. CuO/Cu_2O composite nanowires (NWs) were synthesized on Cu TSV using thermal oxidation. The growth and physical properties of CuO/Cu_2O composite NWs are discussed. The field emission of CuO/Cu_2O composite NWs is examined in detail.

Experimental

A conventional TSV process mainly comprises a photolithography process, a via etching process, isolation/barrier/seed deposition, Cu plating (via filling), chemical mechanical polishing (CMP), temporary bonding (handle carrier), thinning, and de-bonding. The proposed fabrication process has fewer steps (lacking the CMP, temporary bonding, and de-bonding processes of conventional TSV), reducing cost. **Figure 1** schematically depicts the growth and processing steps of the proposed Cu TSV process.

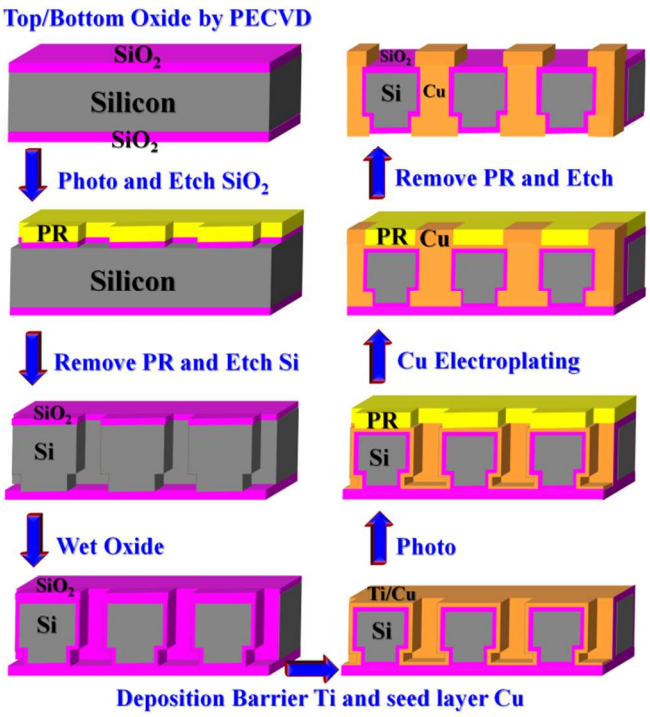

Fig. 1 Schematic diagram of fabricated Cu TSV processes and steps.

Before top-down Cu TSV plating, a 1-μm-thick SiO_2 layer was grown on the front and back surfaces of 6-inch (15.24 cm) Si (100) wafer (thickness = 300μm) as an etching barrier layer. Then, photolithography was applied to define the via pattern. In the silicon via (SV) steps, a 1-μm-thick SiO_2 layer was etched under C_4F_8 (45 sccm) plasma with O2 (8 sccm) for ~15 min. For the TSV process, inductively coupled plasma (ICP) of reactive-ion etching (RIE) was used with the following etching conditions: a flow gas of SF_6 (400 sccm) and O_2 (10.5 sccm), a substrate temperature of -110 °C, an etching time of 90 min, an electrode gap of 7 cm, an ICP power of 1300 W, and a chamber pressure of 15 mTorr. The SF_6 and O_2 gases are used to remove the Si and oxide Si via sidewall, respectively. The SiO_2 isolation layer, Ti adhesion layer, and Cu seed layer were subsequently deposited on the surface of the SV and wafer. A negative-type photoresist was spin-coated onto the Cu/Ti/SiO_2/SV substrate, and then standard photolithography was used to define the bump.

For the electroplating of copper, the wafer was vertically positioned in a 60-mL mixture solution with 40 mL of $CuSO_4$ and 20 mL of H_2SO_4 and HCl, and then electroplated and heated at 90 °C for 5 h. CuO/Cu_2O composite NWs were synthesized in ambient air using annealing at 500 °C for 6 h. The morphology, crystallinity, and optical properties were measured using field-emission scanning electron microscopy (FESEM, JEOL JSM-7000F), transmission electron microscopy (TEM, JEOL JEM-2100F), X-ray diffraction (XRD, Siemens D5000) and photoluminescence (PL) spectroscopy (Jobin Yvon-Spex Fluorolog-3). The current-voltage (I-V) and field emission measurements were conducted using a high-voltage sourcemeter (Keithley 237) at room temperature.

Results and Discussion

Figures 2(a) and **2(b)** show top-view and cross-sectional FESEM images, respectively, of the Si substrate etched with a square pattern (side length: 80 μm). This high-density TSV square pattern is uniform. The gap between TSVs is ~80 μm. The side length and depth of the SV were about ~80 μm and ~280 μm, respectively. **Figures 2(c)** and **2(d)** show the top-view and cross-sectional optical microscopy images, respectively, of the top-down Cu TSV plating. The TSV color is that of Cu metal. Cu uniformly filled each TSV during electroplating. These results demonstrate the feasibility of the proposed Cu TSV fabrication process.

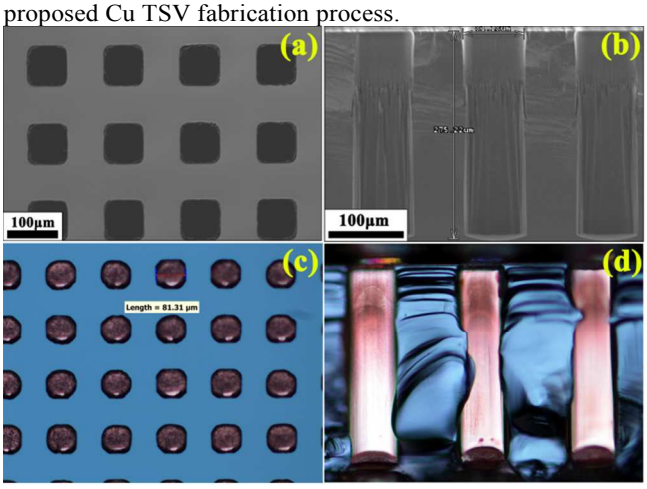

Fig. 2(a) Top view and **(b)** cross-sectional FE-SEM images of TSV, **(c)** top view and **(d)** cross-sectional optical microscope image of Cu TSV plating.

Figure 3(a) presents the etching aspect ratio versus side length curve of the square pattern. The etching ratio increased with increasing square side length. The average diameter and length of the SV varied significantly at a given etching temperature profile and an etching time of 90 min. The inset image shows that the aspect ratio of ICP-RIE-etched silicon is restricted with (I) neutral shadowing, (II) charging, and (III) conduction limit.[27] High-aspect ratio silicon trenches are widely applied in trench capacitors, vertical transistors, microelectromechanical systems, and shallow trench isolation. **Figure 3(b)** shows the resistance (~1.2 mΩ) of a single Cu TSV measured at various current levels. The calculated resistivity ρ of a single Cu TSV is ~2.3×10^{-8} Ω·m, which is higher than that of a Cu block (1.7×10^{-8} Ω·m) due to the structure of the Cu plating being looser.[25-26]

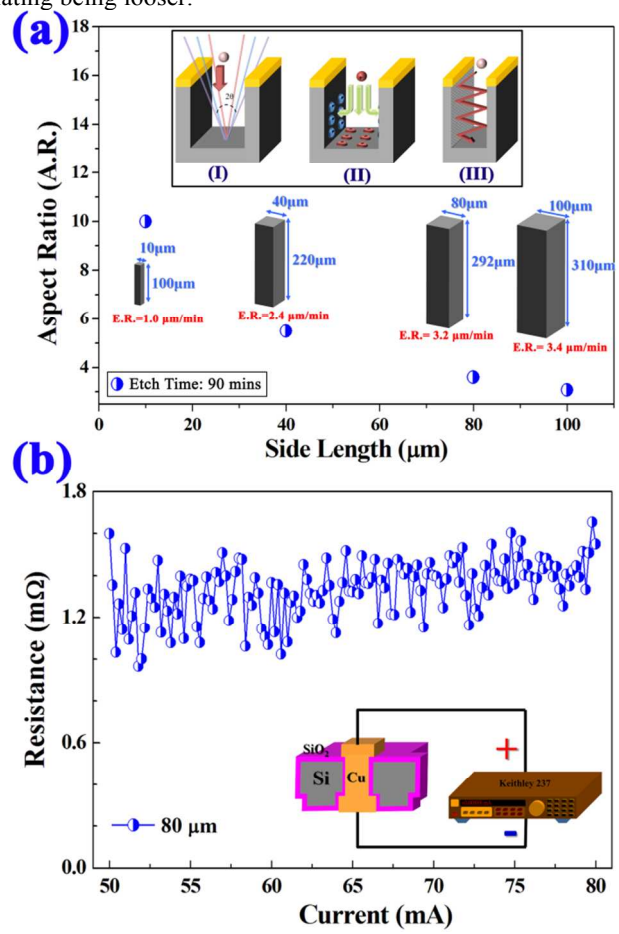

Fig. 3(a) Drawn plot of etching aspect ratio vs. side length of square pattern, insert images depicts ICP-RIE etching silicon limitation. **(b)** Measured resistance of single Cu TSV at various current.

Figures 4(a)-4(c) show cross-sectional FESEM images of the CuO/Cu_2O composite NWs. High-density NWs were grown on the top portion of the Cu TSV. The average diameter and length of the NWs are ~30 nm and ~10 μm, respectively. **Figure 4(d)** shows the energy-dispersive X-ray (EDX) spectroscopy results of the CuO/Cu_2O composite NWs, which indicate that the NWs contained Cu and O. The Cu-to-O peak ratio is 3:2, which indicates that Cu is richer than O and form CuO and Cu_2O.

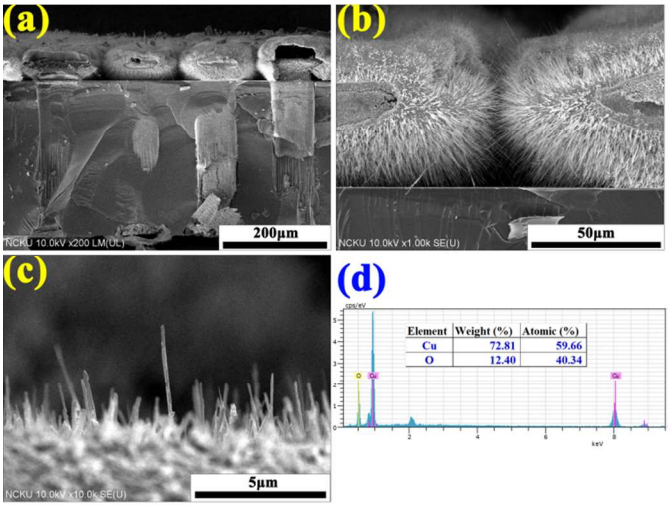

Fig. 4(a)-(c) Cross-sectional FE-SEM images and **(d)** EDX spectroscopy of CuO/Cu_2O composite NWs fabricated by thermal oxidation.

Figure 5(a) shows the XRD θ/2θ-scan pattern of the CuO/Cu_2O composite NWs. The XRD peaks demonstrate that the NWs have the CuO monoclinic and Cu_2O cubic crystalline structures (JCPD card no. 89-2531 and 05-0667, respectively). The CuO ($\bar{1}11$) and Cu_2O (111) peaks are much more intense than the other peaks.

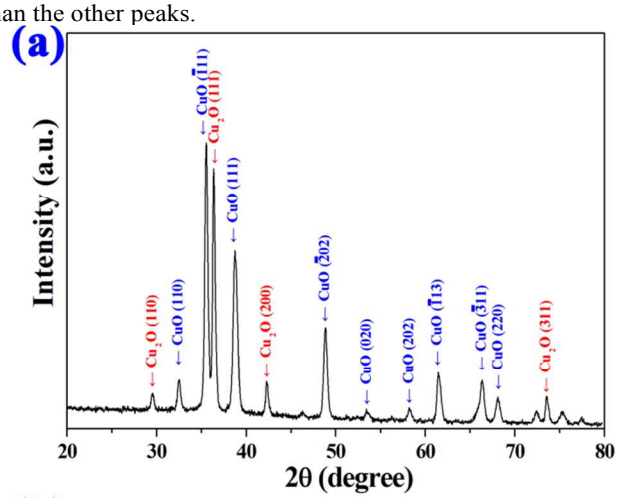

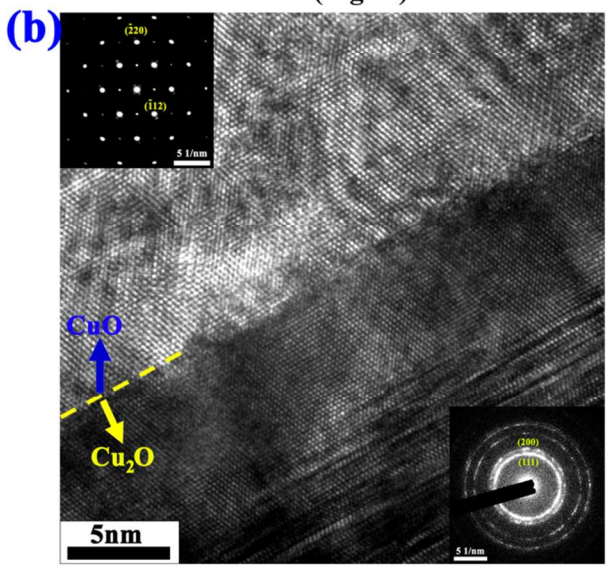

Fig. 5(a) XRD pattern and **(b)** HR-TEM of CuO/Cu_2O composite NWs. The inset displays SAED images.

Figure 5(b) shows a high-resolution (HR)-TEM image of the bottom portion of NWs, showing the CuO/Cu_2O interface. The top and bottom side layers are CuO and Cu_2O, respectively. The top and bottom inset images show the selected area electron diffraction (SAED) patterns of the CuO and Cu_2O layers, respectively. These diffraction patterns verify the single-crystal monoclinic structure of CuO and the polycrystalline cubic structure of Cu_2O. The SAED patterns of CuO and Cu_2O are consistent with the XRD results.

The Cu TSV was heated in the atmosphere at 500 °C. The various thermal oxidation temperatures have been used. The temperature 500°C is optimization experiment condition for longer length of CuO/Cu_2O composite NWs. According the past thermal oxidation reports, The CuO NWs only grow within the temperature range 350~700°C and this study is compatible with previous reports.[28-30] The atmospheric oxygen reacted with the Cu TSV, whose surface quickly oxidized to CuO. The oxygen diffused downward through the CuO layer and then reacted with the Cu TSV. The Cu atoms of the Cu TSV diffused upward through the CuO layer and reacted with atmospheric oxygen to form CuO.[17] The thickness of CuO increased with heating time due to the interdiffusion of oxygen and Cu atoms. When the CuO layer thickness increased to around several μm, the oxygen and Cu atom interdiffusion ratio decreased, slowing the increase of the CuO layer thickness. Because thick CuO acts a barrier layer, there was insufficient oxygen diffusion near the Cu TSV region, leading to the formation of the Cu_2O layer.

There is compressive stress between the Cu and CuO layers due to their lattice mismatch. The stress can be released by the formation of a rough morphology, creating nucleation sites for subsequent CuO/Cu_2O composite NWs. However, a stress-driven mechanism has been widely used to illustrate Cu NWs growths by Cu thermal oxidation synthesize. A previous study showed that the NW growth mechanism is likely stress-driven grain-boundary diffusion.[30-32] The CuO/Cu_2O interface drives outwardly the grain-boundary diffusion of Cu ions. The interfacial strain correlatives with the solid-state phase transformation of CuO/Cu_2O interface. Therefore, the chemical reactions for the CuO/Cu_2O composite NWs grown on top of the Cu TSV are:

$2Cu + O_2 \rightarrow 2CuO$
$4Cu + O_2 \rightarrow 2Cu_2O$
$2Cu_2O + O_2 \rightarrow 4CuO$

Figure 6(a) shows a schematic diagram of the field emission measurement of the CuO/Cu_2O composite NWs. The cathode electrode was connected to the Cu TSV, which acted as an electron channel. Electrons were then emitted from the CuO/Cu_2O composite NWs. **Figure 6(b)** shows the field emission of the CuO/Cu_2O composite NWs measured at room temperature in the dark. The field emission turn-on field of the CuO/Cu_2O composite NWs was 4.7 V/μm, which is comparable to previously reported values, as shown in **Table 1**. The field emission is described by the Fowler-Nordheim (F-N) equation:

$$J = \frac{a\beta^2 E^2}{\phi}\exp\left(\frac{-b\phi^{3/2}}{\beta E}\right)$$

where J is the current density (A/m^2), $a = 1.54\times10^{-6}$ (AeV/V^2), β is the field enhancement factor, E is the applied electric field, ϕ is the work function (eV), and $b = 6.83\times10^3$ ($V/\mu m_e V^{-3/2}$).

The F-N plot is shown in the inset of **Fig. 6(b)**. The work function of CuO is 5.31 eV. Enhancement factor β is ~2092, as calculated from the curve slope.

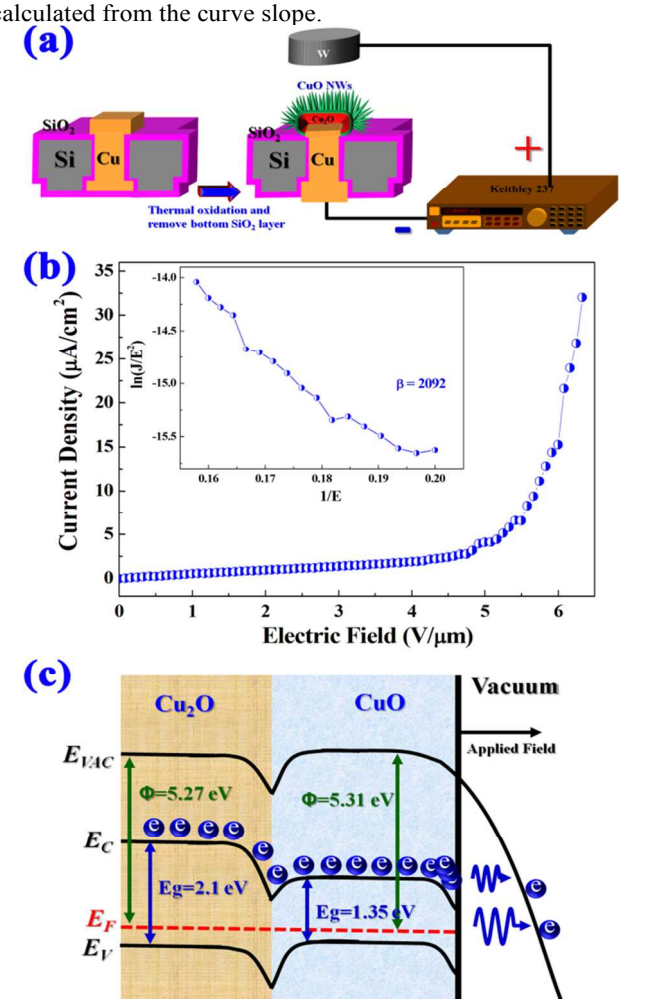

Fig. 6(a) Schematic diagram of the configuration for field-emission measurements. **(b)** Field emission property of CuO/Cu_2O composite NWs, insert image F–N plot of $ln(J/E^2)$ vs. $1/E$. **(c)** Schematic band diagram of CuO/Cu_2O composite NWs in an applied field.

Figure 6(c) shows the band diagrams of CuO/Cu_2O composite NWs in an applied field. The work function ϕ of Cu_2O is 5.27eV, which is close to that of CuO (5.31 eV); however, the bandgap of Cu_2O (~2.1 eV) is larger than that of CuO (1.35 eV). During the fabrication process, the dense surface states should be introduced between Cu_2O and CuO interface. The bands would align and bend to a position relative to surface states of Cu_2O and CuO by Fermi level pinning effect. The electrons were supplied from the electrical power and then passed through the Cu TSV to the Cu_2O region, which form electrons flow. A large number of electrons accumulated in the CuO region, and tunneled from the conduction band (E_C) of the CuO region to the vacuum level (E_V) with an applied field.

Conclusions

A Cu TSV fabrication process that does not require CMP, temporary bonding, and de-bonding processes was developed. Uniform square TSVs with a side length of ~80 μm and a depth of ~280 μm were fabricated. The SiO_2 isolation layer, Ti adhesion layer, and Cu seed layer were subsequently deposited. Cu filled in the TSVs during electroplating. High-density CuO/Cu_2O composite NWs were grown on the Cu TSV using thermal oxidation at 500 °C in ambient for 5 h. The field emission turn-on field and enhancement factor β of the CuO/Cu_2O composite NWs were 4.7 V/μm and ~2902, respectively.

Acknowledgments

The authors would like to thank the Ministry of Science and Technology of the Republic of China, Taiwan, for financially supporting this research under Contract No. MOST 103-2221-E-024-016-

Notes and references

[a] *Department of Electrical Engineering, National University of Tainan, Tainan 700, Taiwan, ROC. Fax: +886-6-2602305; Tel: +886-6-2606123 #7785; E-mail: clhsu@mail.nutn.edu.tw*

[b] *National Nano Device Laboratories, Tainan 741, Taiwan, ROC; E-mail: tj.Hsueh@gmail.com*

Tab. 1 Comparative Field emission performance parameters of this work and conventional CuO 1-D nanostructures reports.

1-D material	Synthesize	Length (μm)	Diameter (nm)	*d* (μm)	$E_{turn\text{-}on}$ (V/μm)	β	Ref.
CuO/Cu_2O Nanowire	**Cu TSV/atmosphere/500°C**	**~10**	**~30**	**100**	**4.7**	**2092**	**This work**
CuO nanowire	Cu plate/atmosphere/390°C	30	60 ± 15	150	3.5	1570	7
CuO nanofiber	nano-Cu nuclei/atmosphere/500°C	8	50	100	6~7		11
CuO Nanoneedle	Cu substrate/atmosphere/700°C	10	30~50	100	0.5		12
CuO nanowire	Cu plate/atmosphere/350°C		30	150	3.7		13
CuO straw-like	Cu foils/H_2O_2 solution/60°C	200~300	100~200	200	2.8	1100	14
CuO nanobelt	Cu foils/NaOH, $(NH_4)_2S_2O_8$ solution	10	20~50		18		15
CuO nanowire	Cu film/$NaClO_2$, NaOH/70°C	0.5~0.8		110	3.6		16
CuO nanoneedle	Cu foils/Zn(NO3), $C_6H_{12}N_4$/95°C	1.8	45	170~200	0.85		17
CuO nanoneedle	nano-Cu plate/atmosphere/700°C	10	25~35	100	9.7	667	18
CuO nanowire	Cu plate/atmosphere/450°C	40	80~100	100	2		19
CuO nanowire	Cu film/atmosphere/450°C	2.5	70	160	4.5	1610	20
CuO nanowire	Cu film/atmosphere/450°C	14.5	40	0.8		330	21
CuO:Zn nanowire	Cu film/atmosphere/450°C	3.5	80	140	4.1	876	22

1 X. C. Jiang, T. Herricks, Y. N. Xia, *Nano Lett.* 2002, **2**, 1333.
2 L. F. Gou, C. J. Murphy, *Nano Lett.* 2003, **3**, 231.
3 B. D. Yuhas, P. D. Yang, *J. Am. Chem. Soc.* 2009, **131**, 3756.
4 J. T. Zhang, J. F. Liu, Q. Peng, X. Wang, Y. D. Li, *Chem. Mat.* 2006, **18**, 867.
5 H. T. Hsueh, T. J. Hsueh, S. J. Chang, F. Y. Hung, T. Y. Tsai, W. Y. Weng, C. L. Hsu, B. T. Dai, *Sens. Actuator B-Chem.* 2011, **156**, 906.
6 A. Dienst, M. C. Hoffmann, D. Fausti, J. C. Petersen, S. Pyon, T. Takayama, H. Takagi, A. Cavalleri, *Nat. Photonics*, 2011, **5**, 485.
7 Y. W. Zhu, T. Yu, F. C. Cheong, X. J. Xui, C. T. Lim, V. B. C. Tan, J. T. L. Thong, C. H. Sow, *Nanotechnology*, 2005, **16**, 88.
8 Y. Wang, R. Q. Shen, X. Y. Jin, P. Zhu, Y. H. Ye, Y. Hu, *Appl. Surf. Sci.* 2011, **258**, 201.
9 C. T. Hsieh, J. M. Chen, H. H. Lin, H. C. Shih, *Appl. Phys. Lett.* 2003, **82**, 3316.
10 R. V. Kumar, Y. Diamant, A. Gedanken, *Chem. Mat.* 2000, **12**, 2301.
11 C. T. Hsieh, J. M. Chen, H. H. Lin, H. C. Shih, *Appl. Phys. Lett.* 2003, **83**, 3383.
12 Y. L. Liu, L. Liao, J. C. Li, C. X. Pan, *J. Phys. Chem. C*, 2007, **111**, 5050.
13 W. Zhu, A. M. Moo, T. Yu, X. J. Xu, X. Y. Gao, Y. J. Liu, C. T. Lim, Z. X. Shen, C. K. Ong, A. T. S. Wee, J. T. L. Thong, C. H. Sow, *Chem. Phys. Lett.* 2006, **419**, 458.
14 D. J. Shang, K. Yu, Y. S. Zhang, J. W. Xu, J. Wu, Y. Xu, L. J. Li, Z. Q. Zhu, *Appl. Surf. Sci.* 2009, **225**, 4093.
15 J. Chen, N. Y. Huang, S. Z. Deng, J. C. She, N. S. Xu, W. X. Zhang, X. G. Wen, S. H. Yang, *Appl. Phys. Lett.* 2005, **86**, 151107.
16 W. Y. Sung, W. J. Kim, S. M. Lee, H. Y. Lee, Y. H. Kim, K. H. Park, S. Lee, *Vacuum*, 2007, **81**, 851.
17 R. C. Wang, C. H. Li, *Cryst. Growth Des.* 2009, **9**, 2229.
18 Y. L. Liu, L. Zhong, Z. Y. Peng, Y. B. Song, W. Chen, *J. Mater. Sci.* 2010, **45**, 3791.
19 Y. W. Zhu, C. H. Sow, J. T. L. Thong, *J. Appl. Phys.* 2007, **102**, 114302.
20 H. T. Hsueh, T. J. Hsueh, S. J. Chang, T. Y. Tsai, F. Y. Hung, S. P. Chang, W. Y. Weng, B. T. Dai, *IEEE Trans. Nanotechnol.* 2011, **10**, 1161.
21 P. R. Shao, S. Z. Deng, J. Chen, J. A. Chen, N. S. Xu, *J. Appl. Phys.* 2011, **109**, 023710.
22 T. Y. Tsai, C. L. Hsu, S. J. Chang, S. I. Chen, H. T. Hsueh, T. J. Hsueh, *IEEE Electron Device Lett.* 2012, **33**, 887.
23 H. R. Khan, D. Mamaltly, D. Vasileska, *IEEE Trans. Electron Devices*, 2008, **55**, 743.
24 J. Kim, J. S. Pak, J. Cho, E. Song, J. Cho, H. Kim, T. Song, J. Lee, H. Lee, K. Park, S. Yang, M. S. Suh, K. Y. Byun, J. Kim, *IEEE Trans. Compon. Pack. Manuf. Technol.* 2011, **1**, 181.
25 C. H. Chiang, L. M. Kuo, Y. C. Hu, W. C. Huang, C. T. Ko, K. N. Chen, *IEEE Electron Device Lett.* 2013, **34**, 671.
26 Y. J. Chang, C. T. Ko, T. H. Yu, C. H. Chiang, K. N. Chen, *IEEE Electron Device Lett.* 2013, **34**, 435.
27 L. Zheng, L. Ling, X. F. Hua, G. S. Oehrlein, E. A. Hudson, *J. Vac. Sci. Technol. A*, 2005, **23**, 634.
28 S. L. Cheng, M. F. Chen, *Nanoscale Res. Lett.* 2012, **7**, 119.
29 G. Filipic, U. Cvelbar, *Nanotechnology*, 2012, **23**, 194001.
30 Q. B. Zhang, K. L. Zhang, D. G. Xu, G. C. Yang, H. Huang, F. D. Nie, C. M. Liu, S. H. Yang, *Prog. Mater. Sci.* 2014, 60, 208.
31 L. Yuan, Y. Q. Wang, R. Mema, G. W. Zhou, *Acta Mater.* 2011, **59**, 2491.
32 Q. B. Zhang, J. X. Wang, D. G. Xu, Z. X. Wang, X. H. Li, K. L. Zhang, *J. Mater. Chem. A*, 2014, **2**, 3865.